Estuaries Vol. 26, No. 6, p. 1401–1415 December 2003

Variation in Surface Turbulence and the Gas Transfer Velocity over a Tidal Cycle in a Macro-tidal Estuary

CHRISTOPHER J. ZAPPA*, PETER A. RAYMOND†, EUGENE A. TERRAY, and WADE R. MCGILLIS

Woods Hole Oceanographic Institution, Applied Ocean Physics and Engineering, Woods Hole, Massachusetts 02543

ABSTRACT: The gradient flux technique, which measures the gas transfer velocity (k), and new observational techniques that probe turbulence in the aqueous surface boundary layers were conducted over a tidal cycle in the Plum Island Sound, Massachusetts. Efforts were aimed at testing new methods in an estuarine system and to determine if turbulence created by tidal velocity can be responsible for the short-term variability in k. Measurements were made during a low wind day, at a site with tidal excursions of 2.7 m and a range in tidal velocity of nearly 1 m s^{-1}. Estimates of k using the gradient flux technique were made simultaneously with the Controlled Flux Technique (CFT), infrared imagery, and high-resolution turbulence measurements, which measure the surface renewal rate, turbulent scales, and the turbulent dissipation rate, respectively. All measurements were conducted from a small mobile catamaran that minimizes air- and water-side flow distortions. Infrared imagery showed considerable variability in the turbulent scales that affect air-water gas exchange. These measurements were consistent with variation in the surface renewal rate (range 0.02 to 2 s^{-1}), the turbulent dissipation rate (range 10^{-7} to 10^{-5} W kg^{-1}), and k (range 2.2 to 12.0 cm hr^{-1}). During this low wind day, all variables were shown to correlate with tidal speed. Taken collectively our results indicate the promise of these methods for determining short-term variability in gas transfer and near surface turbulence in estuaries and demonstrate that turbulent transport associated with tidal velocity is a potentially important factor with respect to gas exchange in coastal systems.

Introduction

Rivers and estuaries receive a steady input of natural and anthropogenic constituents from land. They are also sites of active processing, effectively altering the amount, timing, and form in which land-derived and anthropogenic constituents are exported to the open ocean. Many of these natural and anthropogenic constituents have a gas phase, and the mechanics of gas exchange is directly relevant to the health and biogeochemical budgets of these systems. The transport of CO_2 and oxygen across the interface, or the exchange of volatile pollutants such as polychlorinated biphenyls (PCBs), polycyclic aromatic hydrocarbons (PAHs) and mercury ($Hg^0_{(g)}$) are important processes affecting the overall resilience of these ecosystems.

Because of the difficulties inherent in direct determination of gas exchange, studies rely on models for the gas flux. The air-water flux (F) of a slightly soluble gas can be parameterized as the product of its concentration difference between the bulk and surface water and the gas transfer velocity, k, which embodies the details of the turbulence-mediated transfer,

$$F = k\Delta c = k(C_w - sC_a), \quad (1)$$

where the solubility coefficient, s, is a function of temperature and salinity, Δc is the difference in gas concentrations between the bulk water (C_w) and the surface water in equilibrium with the air (sC_a), and C_a is the gas concentration in air. Since field measurements of this concentration difference for most gases are obtained readily in rivers and estuaries, the goal from a modeling perspective has been to develop parameterizations of the gas transfer velocity.

For slightly soluble gases, the greatest resistance to transport resides in a thin aqueous mass boundary layer (MBL) at the air-water interface in which molecular diffusion dominates (Jähne and Haußecker 1998). The magnitude of k is determined by diffusion through this spatially and temporally varying MBL, whose thickness is a function of near-surface turbulence and molecular diffusivity and is on the order of 10–100 μm. Both boundary layer models and dimensional analysis show that increasing turbulence levels will decrease the MBL thickness, and increase k. Empirical models for k assume that turbulence regulates the exchange and use bulk properties (e.g., wind speed) that may control air-water interfacial turbulence.

* Corresponding author current address: Lamont-Doherty Earth Observatory of Columbia University, 61 Route 9W, P. O. Box 1000, Palisades, New York 10964; tele: 845/365-8547; fax: 845/365-8157; e-mail: zappa@ldeo.columbia.edu

† Current Address: Yale University, School of Forestry and Environmental Studies, 205 Prospect Street, New Haven, Connecticut 06511.

While measurement options and models exist for choosing a value for the gas transfer velocity, the determination of k is difficult to constrain, resulting in a large uncertainty when estimating the exchange of any gas in aquatic or marine systems, particularly river and estuary systems (Raymond and Cole 2001). The ability to accurately measure and predict atmospheric exchange is limited by a lack of understanding of the mechanisms controlling k.

The variability in k for the estuarine environment is a result of the interaction of mechanisms forcing the generation of turbulence that affect the MBL within a given system. In the open ocean, observations show a dependence of k on wind speed (Smethie et al. 1985; Watson et al. 1991; Wanninkhof et al. 1993), and considerable effort has gone into determining an empirical relationship (Liss and Merlivat 1986; Wanninkhof 1992; Wanninkhof and McGillis 1999), since the wind stress at the ocean surface plays a central role in the generation of turbulence through the transfer of momentum to waves and currents. For a wind-driven system, turbulence is generated near the air-water interface primarily through shear, buoyancy, or large- and micro-scale wave breaking. Less dependence is observed under low wind speed conditions since buoyancy may dominate the production of turbulence in the near-surface layer (Soloviev and Schlüssel 1994) and under conditions of surface contamination by thin organic films (Frew 1997). In streams, the generation of turbulence by friction due to flow over the bottom and side topography, with varying roughness, may dominate. The turbulence, in turn, is transported to the MBL at the air-water interface. k varies with hydraulic characteristics such as depth, H, and current velocity, V, and has been semi-empirically modeled (O'Connor and Dobbins 1958; Langbein and Durum 1967; Wilcock 1984).

Rivers and estuaries represent a case in which both wind forcing and boundary friction generate turbulent energy (e.g., Cerco 1989; MacIntyre et al. 1995). Laboratory measurements of transfer rates in rivers for combined wind- and bottom-shear induced turbulence have suggested that the transfer velocity transitions at a critical value for the wind stress and that the processes within each regime are cumulative (Chu and Jirka 1995). The situation is further complicated by the time dependence of the tidally-driven currents and changes in fetch, water depth, or stratification that have spatial heterogeneity in most river-estuary systems.

The complex interplay of wind speed and hydraulic conditions is illustrated in Raymond and Cole (2001) where empirically derived model parameterizations of k show the large potential variability in k between estuaries of differing scale as well as within a given estuarine system. A limited number of direct studies exist that report gas transfer velocities in estuaries using methods such as natural tracers, purposeful tracer additions, and floating domes. These studies offer a large range of k for rivers and estuaries, and various wind speed parameterizations have been proposed based upon these data (e.g., Cole and Caraco 1998; Raymond and Cole 2001). At a given wind speed, measurements of k have been shown to vary by a factor of 2–12. The degree to which this variability is due to inherent differences in the various measurement techniques, or to temporal and spatial variability in the exchange processes, is unknown. It is interesting to note that the floating dome studies, which operate at smaller temporal and spatial scales, tend to report more variability at a given site. One point is to determine if this variability is the direct result of the variation in surface hydrodynamics due to tidal forcing at a given wind speed.

In order to determine the relative role of tidal and wind forcing in controlling k over a wide range of environmental conditions, it is imperative to understand the effect that near-surface turbulence has on the MBL. The continual replacement of water in the MBL through surface renewal (Danckwerts 1951) has been suggested as a fundamental hydrodynamic process controlling gas exchange and has resulted in a useful conceptual model for k. Surface renewal models describe the continuous random renewal of the aqueous MBL with the bulk water below due to turbulent eddies. The idealized process is one in which renewal is complete and instantaneous. As turbulent eddies renew the surface, bulk water parcels that are not in equilibrium with the atmosphere come in contact with the interface and exchange gas with the atmosphere through diffusion. The faster this renewal occurs, the higher the exchange rate. Surface renewal models predict the gas transfer velocity as

$$k \propto (D/\tau)^{1/2} = (D\lambda)^{1/2} \tag{2}$$

where D is the mass diffusivity, τ is the lifetime of a parcel of water exposed to diffusion at the surface, or alternatively $\lambda = 1/\tau$ is the surface-renewal rate. Because not all renewal eddies produce complete fluid parcel overturning at the surface as described in random-eddy penetration models (Harriott 1962), the MBL thickness varies over space and time as eddies intermittently penetrate the layer. From a conceptual standpoint, the implementation of surface renewal does not rely on knowledge of the turbulence generation mechanism and may prove to be a powerful model that is applicable to the estuarine environment.

In an effort to relate the concept of surface renewal directly to near-surface turbulence, Lamont and Scott (1970) developed a hydrodynamic model based upon viscous eddies characteristic of the shortest time scale. Estimating τ by the Kolmogorov, or dissipative, timescale, $(\nu/\varepsilon)^{1/2}$, the near-surface hydrodynamics are directly proportional to $\varepsilon^{1/4}$, and the gas transfer velocity is expressed as

$$k \propto (\varepsilon\nu)^{1/4} Sc^{-n}, \quad (3)$$

where ε is the turbulent kinetic energy dissipation rate and the Schmidt number, *Sc,* is defined as the ratio of the kinematic viscosity of water, ν, to D. The Schmidt number exponent n varies between ½ (clean surface) and ⅔ (contaminated surface) (Ledwell 1984; Jähne et al. 1987). Surface contamination is known to modify the free surface to behave as a rigid boundary by introducing a tangential stress that works to suppress horizontal motion, and therefore near-surface turbulence and k. As shown in Eq. 3, the transfer velocity scales with the turbulent dissipation rate, a parameter that can be measured in the field. This scaling demonstrates that increasing turbulence intensity will enhance k, and this scaling has been tested with success in the laboratory for varying surface conditions (Asher and Pankow 1986).

The ability to accurately predict k in rivers and estuaries is dependent on our ability to make accurate measurements of the processes occurring in the MBL and on generating extended data sets across a continuum of environmental and hydrographical conditions. Progress in this area can be made by using observational techniques with adequate spatial and temporal resolution to map the variability of transfer velocities, while simultaneously carrying out measurements on the factors affecting the turbulence in the MBL that controls the transfer. We apply recently developed techniques to measure the gas transfer velocity for CO_2, the surface-renewal rate, and the near-surface turbulent dissipation rate at short temporal and small spatial scales in the Parker River estuary of Massachusetts over the course of one semi-diurnal tidal cycle. The measurements were carried out from the mobile Surface Processes Instrument Platform (SPIP), a small research catamaran that enables spatial sampling. Measurements were made during a constant low wind period ($\sim$2 m s^{-1}) in order to focus on the effects of changes in tidal velocity on k. Directly measured surface-renewal rates and turbulent dissipation rates may provide the ability to scale the transfer velocity in estuaries based on the processes that are directly controlling gas flux across the air-water interface.

Methods

Study Area

The Plum Island Sound estuary is a coastal plain estuary in northeastern Massachusetts with average semi-diurnal tides of 2.9 m and a spring-neap range of 2.6–3.6 m. Measurements were performed during a flooding tide through slack tide at one site in the upper Parker River, one of two major rivers within the Plum Island estuary that discharges into the Gulf of Maine. The Parker River estuary is a small 12-km macro-tidal estuary with significant temporal and spatial variation in geometry, bathymetry, density structure, wind stress, freshwater input, and tidal forcing. The upper Parker River and the Plum Island Sound estuaries exhibit large spatial gradients in depth and width, temporal gradients in freshwater discharge and wind speed, and large hourly and spring-neap changes in tidal velocity. These gradients have been demonstrated to cause large spatial and temporal variation in the tidal dispersion coefficient (Vallino and Hopkinson 1998), and are expected to affect the variability of gas exchange.

Platform

The SPIP is a 2.1-m, side-towed, quadruple-hulled research catamaran used to measure the atmospheric gradient of CO_2 very close to the air-water interface. SPIP is shown in Fig. 1 and was boomed from the research boat *Growler* as a comprehensive unit to determine the processes that affect these air-water exchanges. The *Growler* was moored at the study site on the Parker River such that the bow of SPIP was directed into the wind and the flooding tidal flow. SPIP has supporting measurements of atmospheric variables and of the water-side forcing. SPIP measures gradients near the surface with potentially less flow distortion than other boat-mounted instrumentation (comparison using a numerical 2-D flow model). The bow of SPIP has one mast with fixed and traveling atmospheric sensors to implement the gradient flux technique as well as a second mast outfitted with an infrared system for thermal imagery of the water surface and for performing the controlled flux technique.

The atmospheric sensors include a Licor model 6262 closed path non-dispersive infrared (NDIR) sensor that measures CO_2 and water vapor concentrations simultaneously with a resolution, or relative accuracy, of $\pm$0.01 μatm and $\pm$0.02 g kg^{-1}, respectively, and with a response time of approximately 0.1 s based upon the flushing rate through the sensor. A Vaisala HMP 235 sensor measures the mean relative humidity and air temperature. A Gill 2-axis Wind Observer II ultrasonic anemometer

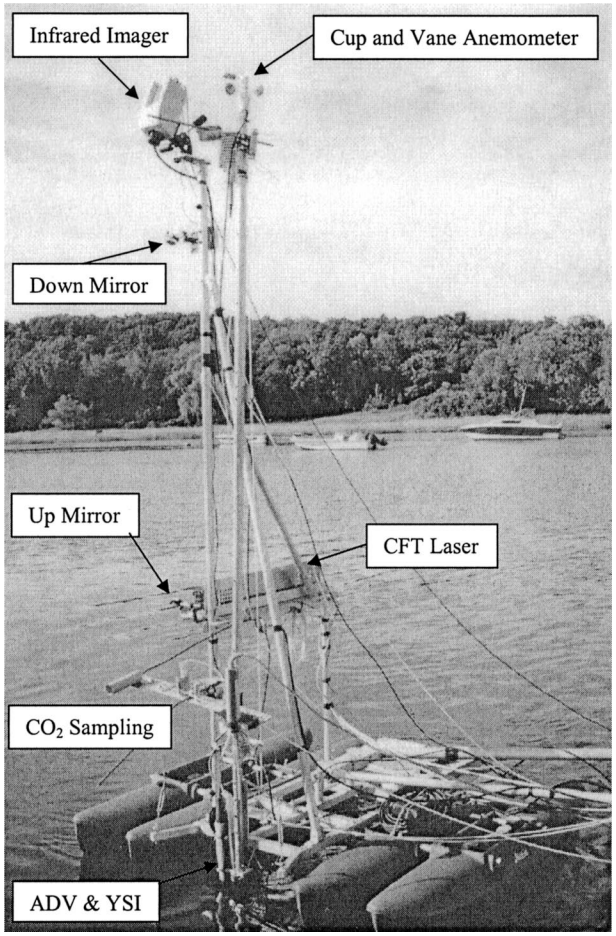

Fig. 1. Picture of the Surface Processes Instrument Platform (SPIP) used for measurements of both the aqueous and atmospheric boundary layers. SPIP has four hulls each measuring 2.1 m in length and two masts each 3.1 m in height. Subsurface instrumentation includes an acoustic Doppler velocimeter (ADV), an acoustic Doppler current profiler (ADCP), salinity, temperature, and pCO_2. Interfacial measurements include an infrared camera and an incident 10.6 μm wavelength CO_2 laser beam. Atmospheric measurements include fixed and profiling wind speed, temperature, relative humidity, water vapor, and carbon dioxide.

and a Met One 034A-L cup anemometer with vane are both used to measure wind speed. The fixed atmospheric sensors are located at the top of the 3.1-m gradient flux mast while a second set of identical sensors is mounted to a vertical traversing system. The gradient flux technique described below outlines the estimation of the CO_2 fluxes from the measured gradients in conjunction with the appropriate scalar transfer coefficients in order to determine the gas transfer velocity from Eq. 1.

The primary waterside measurements include pCO_2, temperature, salinity, tidal flow velocity, current shear, and tidal height. The aqueous pCO_2 is measured using an equilibrated headspace sampled with a Licor 6262 NDIR sensor with an overall system response time of 2 min as determined from laboratory tests. The water temperature and salinity are measured with a YSI model 660XL that was calibrated to within ±0.1°C and 0.1 psu, respectively. A near-surface point measurement of x-, y-, and z-axis velocity components was measured using a Sontek 3-axis acoustic Doppler velocimeter (ADV). Mean tidal flow velocity and turbulent velocity (e.g., energy dissipation rate) statistics were estimated from 15-min records sampled at 25 Hz. A 1200 kHz bottom-tracking Acoustic Doppler Current Profiler (ADCP) deployed from SPIP profiled the water column at 1-s intervals to measure current shear, tidal current, and elevation.

The second 3.1-m mast was outfitted with an infrared (IR) system to implement both imagery of the aqueous thermal boundary layer and the controlled flux technique (CFT). A Merlin MWIR infrared imager was mounted to the top of the IR mast and viewed the surface at a 20° incidence angle. This configuration resulted in a roughly 3 m (vertical) by 3.5 m (horizontal) image size. The noise equivalent temperature difference (or mean resolvable temperature difference) of this model is specified at ±0.02°C. A Synrad model G48–2–28(W) continuous-wave 25-W CO_2 laser operating at 10.6 μm was directed at the water surface from above the tank using a series of 5-cm diameter IR mirrors, as depicted in Fig. 1, and was pulsed for 10 ms with a gating frequency of roughly 0.25 Hz. The laser beam generated heated spots on the water surface in the field of view of the infrared imager roughly 2–3 cm in diameter. For the runs used to determine the decay time from the CFT, the infrared imagery was digitized at a frequency of 20 Hz.

Gradient Flux Technique

The flux of gas through a boundary layer is directly proportional to the concentration gradient that exists within that layer. The mass flux across the aqueous and airside MBLs at the air-water interface is in balance in steady state conditions, even though the gradient may be controlled on either side depending on the gas solubility and transfer rates (Liss 1973; Liss and Slater 1974; McGillis et al. 2000). It follows directly that the flux from the air-water surface must be in balance with the flux through the atmospheric surface layer under homogeneous conditions (Panofsky and Dutton 1984). The gradient flux technique uses vertical profiles of the mean CO_2 concentration, $\bar{c}$, in the atmospheric surface layer (ASL) to estimate the flux of CO_2 across the air-water interface. In the gradient flux technique, the flux is obtained by multiplying the vertical mean gradient of CO_2

in the ASL by the turbulent eddy diffusivity, K_c, such that

$$F = K_c \frac{\partial \bar{c}}{\partial z}, \quad (4)$$

where z is the height above the mean water surface (Businger et al. 1971; Dyer 1974). The eddy diffusivity denotes the effectiveness of transport through the ASL, whose thickness is on the order of 1–10 m. Empirical relationships over land (Businger et al. 1971; Dyer 1974) and the ocean (Edson and Fairall 1998) indicate that there is a similarity between the gradients of scalar quantities such as temperature, specific humidity, and trace scalar constituents such as CO_2. This means that the eddy diffusivities for these quantities behave similarly, and the eddy diffusivity for CO_2, K_c, may be estimated from the diffusivity for other scalars that are measured within the ASL. The eddy diffusivity for CO_2, K_c, is dependent on the stability of the ASL, the height within the ASL, z, and wind speed, and results in a semi-logarithmic profile of $\bar{c}$ when incorporated into Eq. 4. The flux of CO_2 is determined from the semi-logarithmic concentration gradient according to Eq. 4. The flux estimate determined from Eq. 4 is used along with the measurements of the air-water concentration difference to calculate k in Eq. 1.

The profiles are determined using one set of traveling sensors that measure concentrations at various heights within the atmospheric boundary layer. This minimizes the main drawback of the gradient flux technique that requires accurate measurements of the mean scalar quantities in order to resolve concentration gradients. A single set of instruments is used for profiling in order to augment the precision of the measurement since this will eliminate inter-sensor biases. A second set of sensors is held fixed in order to account for the atmospheric variability that occurs over the measurement time. Measurements at each height are averaged for 7 min such that a vertical profile is completed within 30 to 45 min. Open-ocean measurements of water vapor gradients show that the atmospheric variability is a factor of 3 greater than the vertical gradient (McGillis et al. 2001). Subtracting the fixed reference from the traveling measurement, the atmospheric variability can be removed. The small air-sea CO_2 concentration differences on the open ocean limit the gradients in the ASL to the ppb range, which is close to the analytical precision of the gradient flux technique (McGillis et al. 2001).

Since the gradient flux technique relies on mean gradients in the ASL, it offers several advantages in determining air-water fluxes. Other methods, such as purposeful gas addition rely on measurement procedures that result in large temporal and spatial footprints. The gradient flux technique averages over smaller spatial (on the order of 100 m^2) and temporal (on the order of 10 min) scales, which is necessary for sampling processes such as tides. The method works best when the wind is moderate and the stratification within the ASL is minimal. There is greater uncertainty in low wind regimes where the eddy diffusivity is not well understood. At very high winds, spray is generated at the interface, carried into the ASL, and acts as a source for water vapor and a sink for sensible heat. Sources and sinks within the ASL violate the basis for which the flux-profile relationship is constructed and have not been tested reliably. Since the gradient flux technique depends upon the atmospheric boundary layer, some combination of shifting winds and short fetch creates uncertainty in rivers and estuaries. Care was taken to ensure that the measurements reported here were for cases when the flux footprint was over water.

Passive Infrared Imagery and Controlled Flux Technique

Analogous to the MBL, a net heat flux from the water to the atmosphere occurs by molecular conduction through the aqueous thermal boundary layer (TBL) at the surface (Katsaros 1980; Robinson et al. 1984). As a result, the temperature at the water surface, or skin, is less than the bulk temperature immediately below typically by several tenths of a degree Celsius (Schlüssel et al. 1990; Wick et al. 1996; Donlon and Robinson 1997). This thin, gravitationally-unstable TBL is on the order of 10^{-3} m thick or less (McAlister and McLeish 1969; Wu 1971; Hill 1972), and exists for a variety of forcing, including shear-driven (Saunders 1967) and buoyancy-driven (Katsaros et al. 1977) turbulent processes. Free convection dominates during conditions of strong cooling and low wind, and the skin temperature has been observed to be on the order of 1°C less than the bulk (Katsaros 1977). A stable TBL may even develop under intense insolation and low winds where the skin temperature has been suggested to be warmer than the bulk (Katsaros 1980; Soloviev and Schlüssel 1996). Observations at moderate to high wind speeds when wavebreaking and other shear-driven processes dominate suggest that the skin temperature may asymptote to a value that is 0.1°C below the bulk (Donlon et al. 1999). This brief list, though incomplete, demonstrates the range of processes that govern the behavior of the TBL and suggests that its vertical and horizontal structure is quite complex due to the variability of the near-surface tur-

bulence mechanisms and due to the supporting heat flux.

Passive infrared imagery measures the microscale horizontal structure in skin temperature and can be used as a visualization tool for turbulence at water surfaces in rivers and estuaries. An infrared imager is ideally suited to measure the skin temperature because the optical depth of the infrared radiation detected, roughly on the order of 10^{-5} m (McAlister 1964; McAlister and McLeish 1970), is much less than the thickness of the TBL. Recently developed infrared imaging techniques have quantified signatures of thermal variability that result from renewal processes such as large-scale wave breaking (Jessup et al. 1997), microbreaking (Zappa 1999; Zappa et al. 2001a,b), near-surface shear, and free-convective patchiness (Zappa et al. 1998). Measurements show that when the cool skin layer is momentarily disrupted by a breaking wave, the skin temperature of the resulting turbulent wake is approximately equal to the bulk water temperature. As the wake subsides, the skin layer recovers, and the skin temperature returns to its original, cooler value at a rate that increases with net heat flux. Less energetic processes such as intermittent or free convection also produce renewal of the TBL, and have longer timescales of surface renewal than wavebreaking or other shear-driven turbulent processes (Soloviev and Schlüssel 1994; Wick et al. 1996; Zappa et al. 1998). In estuaries, bottom-generated turbulence that diffuses to the air-water interface and wind-generated turbulence will further contribute to the disruption of the TBL. Infrared measurements of the temporal and spatial characteristics of skin temperature variability provide the capability to remotely monitor free-surface turbulence under conditions of constant heat flux or when the heat flux dependence is known.

The controlled flux technique (CFT) (Jähne and Haußecker 1998) uses heat as a proxy tracer for gas to obtain the remote measurement of the surface renewal rate with high spatial resolution and short response times. In the CFT, the water surface is heated with a CO_2 laser (optical depth is roughly 10.5 μm) to produce a spot with a measurable temperature difference that can be tracked within a sequence of infrared images. The MBL resides within the thermal boundary layer described above and is similarly affected by near-surface turbulence. Since the optical depth of the detected infrared radiation is on the order of the mean thickness of the mass boundary layer, disruptions of the TBL observed in the infrared imagery serve as an estimate of the surface renewal within the MBL with bulk water. By tracking the decay of the small, circular (on the order of 10 cm^2) heated parcel of water within the TBL, CFT produces averaged measurements of the surface renewal rate, λ, with a spatial resolution on the order of 1 m^2 and over a period of minutes.

The heated spot is tracked in the infrared imagery to determine the surface renewal rate, λ, which is estimated from the thermal decay of the heated spot as predicted from a surface renewal model. The technique fits the normalized surface temperature, T_N, of the patches tracked to

$$T_N = \frac{h}{\sqrt{h^2 + 4\alpha t}} e^{-\lambda t} \tag{5}$$

where h is the penetration depth that is bound to the optical depth of the CO_2 laser waveband and α is the thermal diffusivity of water. The analytical solution of the one-dimensional unsteady diffusion equation shown in Eq. 5 incorporates a turbulent transport term characterized by statistical renewal of the surface layer by subsurface eddies. In Eq. 5, the distribution of surface renewal is modeled as an exponential, which states that the most probable lifetime of a water parcel at the surface is zero. Other distributions (e.g., log normal or gamma) may prove to give better prediction for the surface-renewal rate. The transfer velocity scales directly with $\sqrt{\lambda}$ such that enhanced surface renewal will elevate gas transfer. The heat transfer velocity is then calculated directly from

$$k_H \propto \sqrt{\alpha\lambda} = \sqrt{\alpha/\tau}. \tag{6}$$

Since both heat and gas are scalars, k_H is believed to scale directly to the gas transfer velocity, k, by

$$k = k_H\left(\frac{Sc}{Pr}\right)^{-n} = k_H(Le)^{-n} \tag{7}$$

where Sc is the Schmidt number, Pr is the Prandtl number, Le is the Lewis number, and n varies between ½ and ⅔ depending upon the cleanliness of the air-water interface.

Previous CFT measurements have provided reliable estimates of k in the laboratory (Jähne et al. 1989; Haußecker et al. 1995). A limitation for the technique may be that not all eddies that affect the MBL and renew the surface are complete and instantaneous, and penetration theory (Harriott 1962) may prove to be more appropriate. The choice of n in Eq. 7 is difficult to determine in natural systems when using this technique. CFT ideally should be complemented with dual-tracer techniques (Clark et al. 1994) or another suitable method for determining the surface condition.

Near-Surface Turbulence

In steady flow with isotropic, fully-developed turbulence, kinetic energy cascades from large eddies

to smaller eddies that finally dissipates through viscosity. This cascade of energy occurs within the inertial subrange, defined as the wavenumber range between the large slow scale of turbulence production, and the small fast scale of molecular dissipation. Under these conditions, the turbulent dissipation rate, or the rate of energy transfer in a turbulent fluid, can be estimated by the magnitude of the wavenumber spectrum in the inertial subrange. The inertial dissipation (ID) method is used to determine the turbulent kinetic energy dissipation rate, ε, as

$$S = \alpha\varepsilon^{2/3}\kappa^{-5/3} \tag{8}$$

where S is the wavenumber spectrum of the fluctuating vertical velocity, w, $\kappa = 2\pi f/V$ is the wavenumber, f is the frequency, and α is Kolmogorov's empirical constant of 0.52.

Measurements of ε were made in the Parker River according to this model for the inertial subrange of the kinetic energy spectrum in Eq. 8 using an ADV. The ADV sampled the three components of water velocity at 25 Hz, 38 cm below the air-water surface. The frequency spectra were measured and corrected for pulse averaging by dividing the measured frequency spectra by the factor $[\sin(\pi f\Delta t)/\pi f\Delta t]^2$. Assuming Taylor's hypothesis of frozen turbulence, the frequency spectra were then converted to wavenumber space by $\kappa = 2\pi f/V$ and ε is calculated directly from Eq. 8. A safe lower bound of the inertial subrange for these data was determined to be 20 rad m^{-1} according to the criterion $\kappa z > 5$. A reasonable upper bound was determined to be 80 rad m^{-1} according to the criterion $\kappa L < 1$, where L is the length scale of the sample volume (L = 1 cm for the ADV used in this study).

For steady-state, homogeneous conditions, the turbulent kinetic energy budget requires that the turbulent dissipation rate is balanced by the sum of shear and buoyant (i.e., stratification) production and the relative contributions of each to ε is determined by the Richardson number, Ri. For instance, the Ri is used to characterize the state of near-surface mixing. For Ri less than a critical value, vertical mixing is expected to occur by shear instability. Since stratification plays a prominent role in the dynamics of estuaries, the turbulent dissipation rate may be affected by the near-surface buoyancy production.

Surfactants are known to modify the boundary condition at the air-water interface. Theoretical arguments suggest that at a clean water surface the fluid is free to undergo tangential straining motions that allow for turbulent eddies to penetrate the MBL and promote k (Ledwell 1984; Jähne et al. 1987). In the presence of surfactants, the air-water interface behaves similar to a solid boundary and the no-slip condition inhibits turbulent motion near the MBL. Laboratory studies have shown that measurements of turbulent velocity fluctuations in the bulk were not representative of mixing within, or very near, the MBL (McKenna and McGillis 2001). Rather, surface divergence, which is a manifestation of surface renewal measured by CFT, showed a high correlation with the gas transfer velocity. Measurements of the turbulent dissipation rate within the interfacial boundary layers are difficult and are more tractable at depths below the surface (the depth of the turbulence measurement >5 cm, depending on the waves).

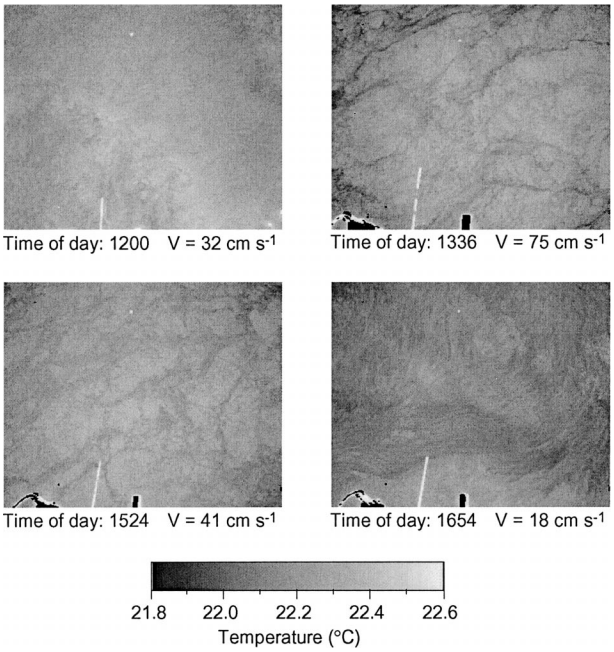

Fig. 2. Examples of infrared images of the water surface at 4 different tidal phases (varying tidal speeds, V, from 18 to 75 cm s^{-1}) on the Parker River on August 4, 2000. These images indicate the microscale structure in temperature variability at the estuary surface that is a direct result of surface renewal governed by near-surface turbulence. During the 5-h experiment, the wind speed was 1.9 ± 0.5 m s^{-1}, relative humidity decreased from 58% to 35%, the air temperature increased from 23.1°C to 25.6°C, and the water temperature was 22.3 ± 0.2°C. The images were taken with the Merlin model MWIR and the image size is roughly 3 m × 3.5 m.

Results

Measurements were obtained at the Parker River from SPIP using an infrared imager, which provides a time series of two-dimensional images of the skin temperature as inferred from the infrared radiance. Figure 2 shows examples of infrared images of the water surface at 4 different tidal phases (varying tidal speeds, V, from 18 to 75 cm s^{-1}). The first example at 1,200 has a smooth appearance

with small-scale spatial variability and slow-moving features during a low-flow regime ($V = 32$ cm s^{-1}). The second example at 1,336 is typical for peak velocity during flood conditions and depicts active and energetic disruption of the skin layer with wide, sweeping regions of strong upwelling of warmer temperature and thin veins of converging cooler temperature. The spatial scale of these upwelling events is on the order of 0.1–1 m and the temporal scale is on the order of 0.1 s during a flow of $V = 75$ cm s^{-1}. The skin temperature differences within the image reach above 0.5°C. The third example follows the peak velocity during flood tide and shows features similar to the second example with similar spatial scales. The system is less energetic as evident by longer timescales for renewal, on the order of 1 s, and wider veins of converging cooler water, probably a result of the lower flow ($V = 41$ cm s^{-1}). The final example ($V = 18$ cm s^{-1}) is similar to the first with a smooth appearance and wispy features of small spatial scale on the order of 1 cm and long temporal scales for renewal on the order of 10–100 s. The spatial and temporal variability of the skin temperature from the infrared imagery provides insight into the evolution over the tidal cycle of the near-surface turbulence that affects the interface and controls the gas transfer.

The surface renewal observed in the infrared imagery of Fig. 2 varied significantly over the tidal cycle and was quantified using CFT. The controlled flux technique is demonstrated in Fig. 3, which compares two sequences of infrared images taken at different phases of the tidal cycle. The top sequence ($V = 32$ cm s^{-1}) corresponds to the first example described in Fig. 2 showing a heated patch produced by the CO_2 laser as it decays over 4 s. The bottom sequence ($V = 63$ cm s^{-1}) was taken between examples 2 and 3 described in Fig. 2 showing a heated patch as it decays over 2 s. The patch is observed to decay quicker for the energetic turbulent regime of the tidal cycle when elevated levels of surface renewal were observed. Two time series of T_N are shown in Fig. 4a for the same examples described in Fig. 3 ($V = 32$ and 63 cm s^{-1}). Assuming the surface cleanliness is constant, the transfer should increase as the tidal speed increases. As the tidal speed increased, T_N decayed more quickly and λ increased. The rate of decay of the heated patch in the infrared imagery varied significantly over the tidal cycle. Figure 4b shows that the surface renewal rate increased with tidal speed and the nine independent estimates of λ ranged from 0.03 to 1.6 s^{-1}.

Lamont and Scott (1970) related surface renewal to the turbulent kinetic dissipation rate by estimating the surface renewal timescale as the Kolmogorov timescale that resulted in Eq. 3. As ε increases, renewal of the surface with bulk water is enhanced as is air-water gas exchange. Figure 5a demonstrates the ID method and shows two spectra of fluctuating vertical velocity that were taken after the peak flood velocity ($V = 71$ and 41 cm s^{-1}). Note that both spectra approach an $f^{-5/3}$ power law in the inertial subrange and that the higher spectral level corresponds to the higher flow at that tidal phase. The magnitude of the dissipation rate follows from Eq. 8, and Fig. 5b shows that higher values of ε occur for higher velocities in the tidal cycle. This suggests that the higher surface renewal observed in Fig. 2 and described by CFT in Figs. 3 and 4 is directly related to the near-surface turbulence. Measurements of dissipation rate in the Parker River estuary show that ε ranged from 10^{-7} to 10^{-5} W kg^{-1} (eight independent samples from spectra). An order of magnitude estimate of ε for the conditions in this estuary were comparable according to the scaling κu_*^3 where $u_* = C_D^{1/2} V$ is the friction velocity, and C_D is the drag coefficient.

The relationship of surface renewal and turbulent dissipation rates to gas transfer and the ability to characterize the estuarine processes that are thought to control gas transfer require high-resolution measurements of k. The Parker River estuary is often supersaturated in CO_2, and for the present study, aqueous pCO_2 concentrations ranged

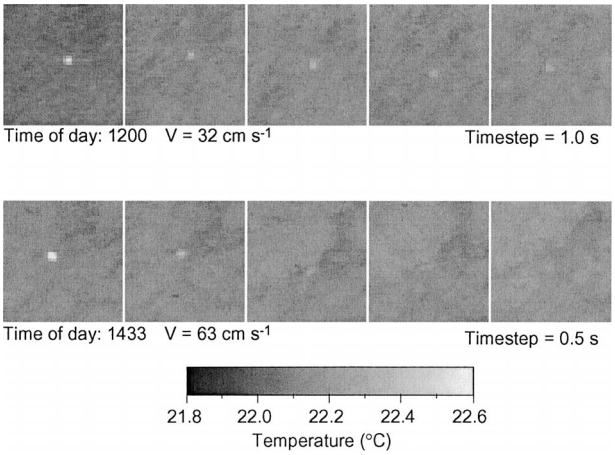

Fig. 3. Comparison of two sequences of infrared images depicting the controlled flux technique (CFT) taken at different phases of the tidal cycle. The top sequence ($V = 32$ cm s^{-1}) corresponds to the first example described in Fig. 2 showing a heated patch produced by the CO_2 laser as it decays over 4 s. The bottom sequence ($V = 63$ cm s^{-1}) was taken between examples 2 and 3 described in Fig. 2 showing a heated patch as it decays over 2 s. The patch is observed to decay quicker for the more turbulent regime of the tidal cycle with elevated levels of surface renewal. The scale of the images are roughly 20 cm $\times$ 20 cm.

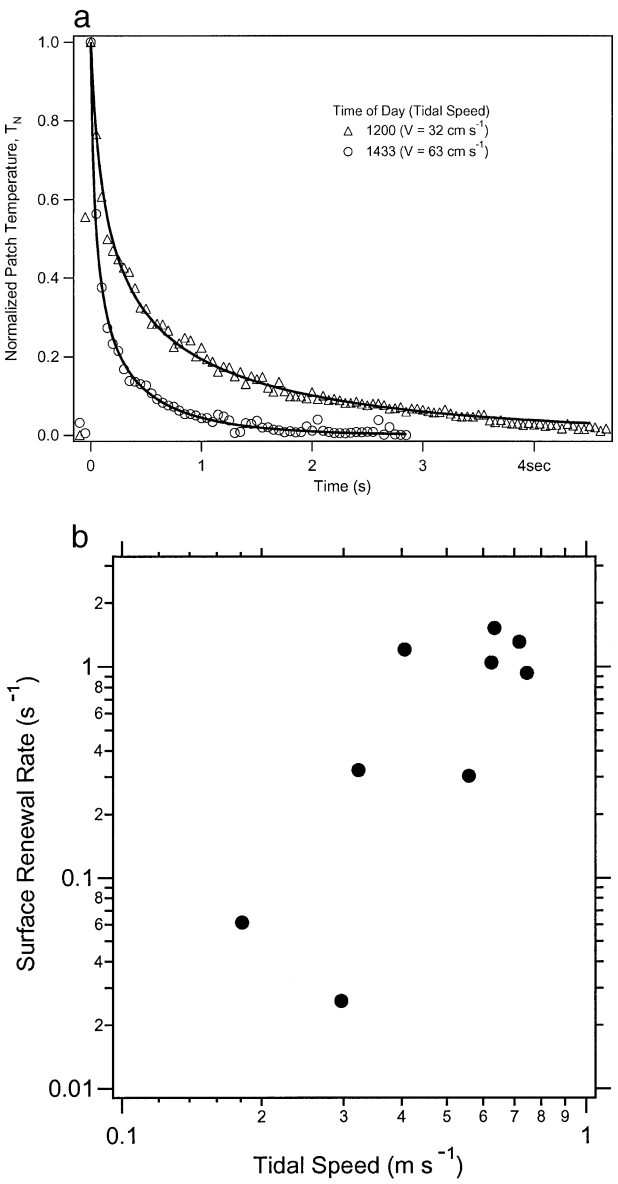

Fig. 4. a) Two time series of the normalized surface temperature, T_N, of the patches tracked by the CFT are shown for the same examples described in Fig. 3 ($V = 32$ and 63 cm s^{-1}). b) Surface renewal rate, λ, determined by CFT versus tidal speed. Assuming the surface cleanliness is constant, as the tidal speed increased, T_N decayed more quickly, and λ increased.

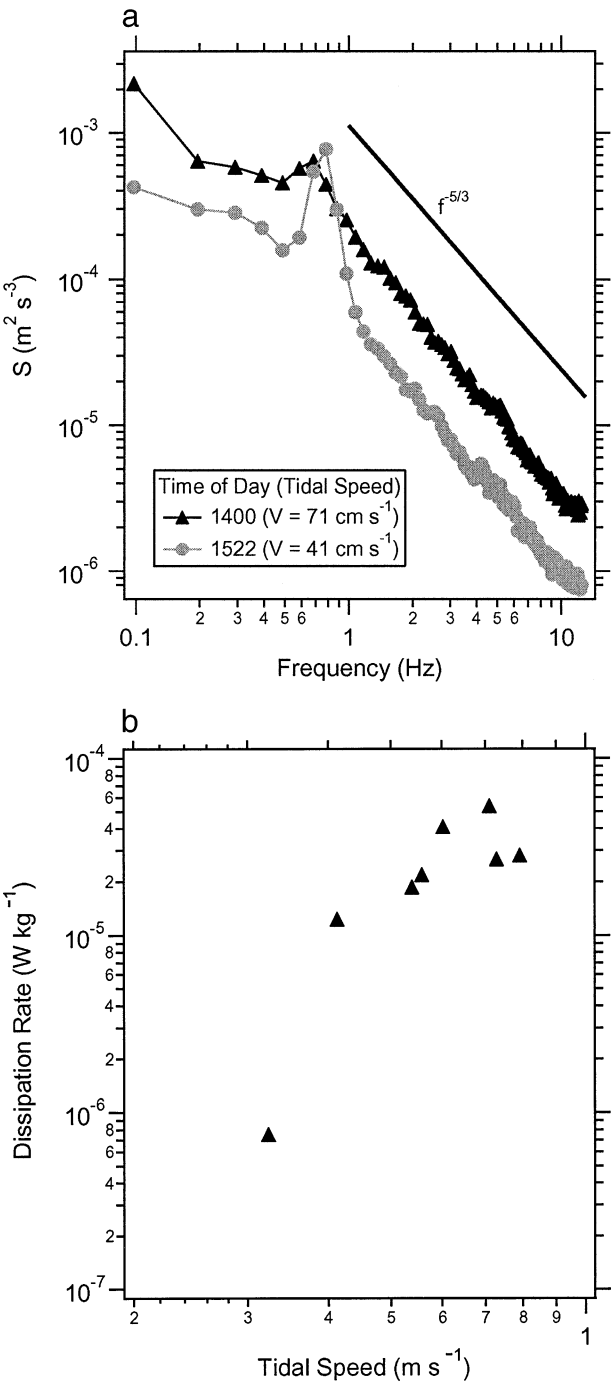

Fig. 5. a) Comparison of two frequency spectra, S, of fluctuating vertical velocity measured from a downward-looking acoustic Doppler velocimeter (ADV) are shown for $V = 71$ and 41 cm s^{-1}. Both spectra show a $f^{-5/3}$ power law dependence in accordance with the inertial dissipation subrange modeled in Eq. 8. b) Turbulent dissipation rate, ε, versus tidal speed. Higher levels of the inertial subrange correspond to higher values of ε, and greater dissipation rates occur for high current speeds observed during the flooding tide.

from just under 3,000 to over 6,000 μatm making it ideal for the gradient flux technique for CO_2 in estuaries. Figure 6a shows the measurements of the fixed and traveling atmospheric pCO_2. The method continually measures the background atmospheric CO_2 concentrations at the fixed reference height, in order to correct for the localized variation in atmospheric CO_2. A single traveling instrument was implemented for profiling in order to eliminate inter-instrument biases that make preci-

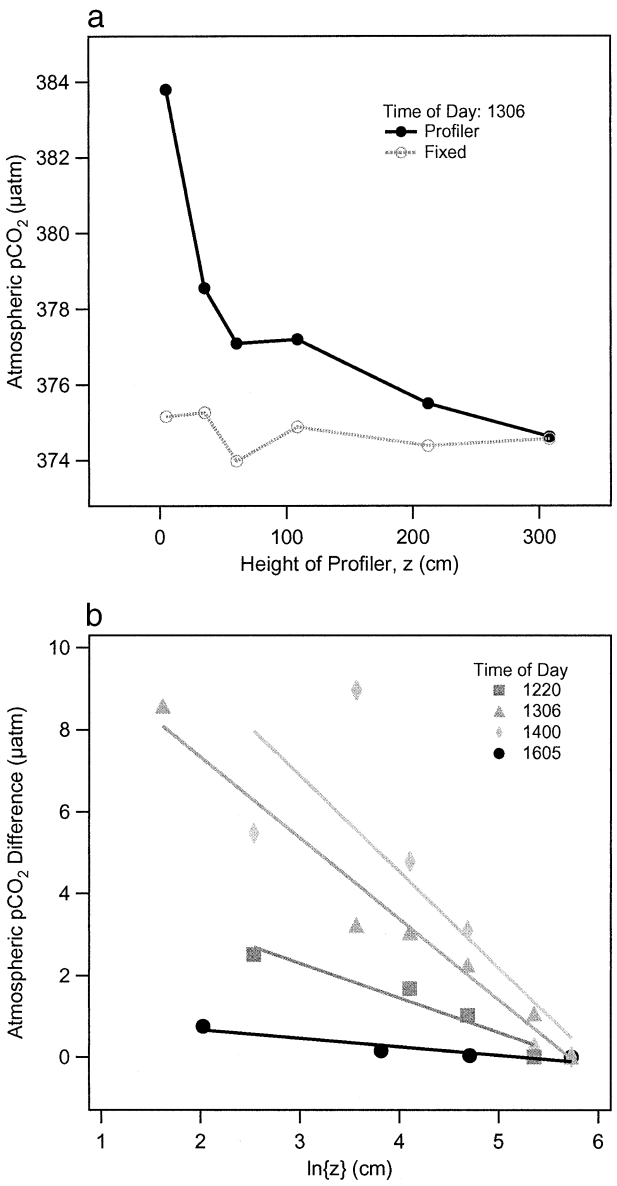

Fig. 6. a) Example of the CO_2 measurements within the ASL and b) a summary of the CO_2 gradients measured on the Parker River estuary. Calibrated CO_2 was measured at the 3 m height using one set of instruments, and a second set of instruments profiled the atmospheric surface layer. The profiling instruments spent 7 min at each height. Simultaneous calibrated measurements made at the top of the mast were subtracted from the profiled measurements. The precision of the gradient is increased by removing the variability of atmospheric CO_2 during the course of a gradient measurement. Using a single instrument to profile avoids inter-instrument biases.

sion profiles difficult. Figure 6b shows the four semi-logarithmic CO_2 gradients in the ASL measured during this study. Note that the atmospheric variability observed at the fixed sensor is accounted for in the profile when determining the gradient, and K_c was determined for the stable ASL. The flux was calculated from the measured atmospheric gradients according to Eq. 4, and the gas transfer velocity determined from Eq. 1 ranged from 2.2 to 12.0 cm hr^{-1}.

Discussion

The significant variability observed in the gas transfer velocity measured on the Parker River over a tidal cycle and under low-wind conditions is related directly to the surface renewal rate and the turbulent dissipation rate. Figure 7 shows k determined from the gradient flux technique as well as λ determined from CFT and ε determined from the ID method over the tidal cycle compared to the tidal speed. The transfer velocity is shown to follow the tidal speed because the wind speed was low and constant (1.9 ± 0.5 m s^{-1}) during the measurement period. Estuarine transfer velocities at low wind speeds similarly track both the turbulence (ε) and surface renewal (λ) generated during the tidal cycle. The measurements of k are consistent with previous results summarized in (Raymond and Cole 2001), though with finer spatial and temporal resolution. Tidal variability leads to significant variation in the near-surface turbulence that directly affects the surface renewal. Similar variations are observed for the gas transfer. The results show that the surface renewal characterized by CFT is consistent with the observations of the spatial and temporal variability of surface renewal observed in the IR imagery of Fig. 2. This surface renewal is tightly coupled to the near-surface dissipation rate, and shown to directly affect the CO_2 gas transfer across the air-water interface.

Surface renewal is the transport of water into the aqueous MBL with the bulk water from below. This renewal is a function of turbulence that exists at or near the water surface. Because gas exchange is also governed by turbulence at the surface, CFT represents an important method for understanding the relationship between turbulence, the processes that generate turbulence, and gas exchange. CFT produced measurements of λ with a spatial resolution on the order of 1.0 m and temporal mean on the order of 100 s. This technique shows the extensive spatial variability of the surface renewal rate in a dynamically evolving estuarine system on short timescales. Since the controlled flux technique is measured within the aqueous MBL, exactly where the gas transfer velocity is controlled for slightly soluble gases such as CO_2, CFT describes the effect that near-surface turbulence has at the air-water interface by the surface renewal process. CFT not only provided a record of the surface renewal rate under all conditions, but also proved to be a powerful complement to the gradient flux technique, which produces results that

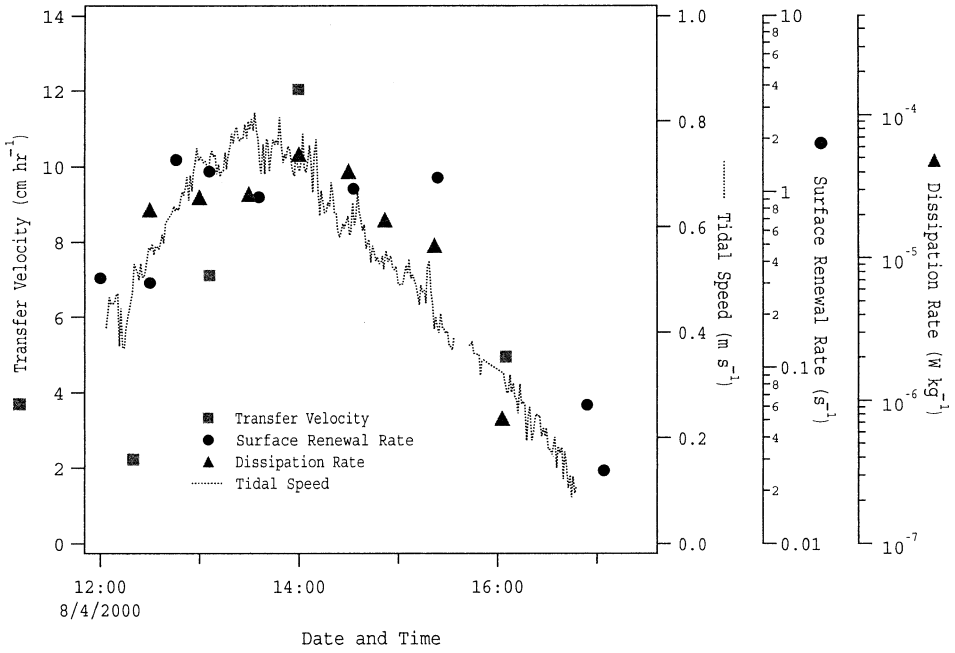

Fig. 7. Results show the transfer velocity measured by the gradient flux technique, surface renewal rate measured by the controlled flux technique (CFT), and the turbulent dissipation rate. Measurements were made during a low wind day (~2 m s^{-1}) on the Parker River Estuary over one-half of a tidal cycle.

are difficult to interpret under no or low wind conditions when tidally generated turbulence dominates.

Previous estimates of λ during laboratory experiments of microscale wave breaking ranged from 1.5 to 7.3 s^{-1} for wind speeds of 4.2 to 9.3 m s^{-1} (Zappa 1999; Zappa et al. 2001b) as well as similar laboratory wind-forced surface renewal rates that ranged from 0.8 to 4.8 s^{-1} for wind speeds of 2.5 to 11.0 m s^{-1} (Haußecker et al. 1995), while open ocean estimates have been reported to range from 1.0 to 1.8 s^{-1} for wind speeds of 3.5 to 6.0 m s^{-1} (Haußecker et al. 1995). The estimates of surface renewal for the Parker River estuary at peak velocity during flood tide are comparable to the lowest wind speeds in the laboratory studies and the open-ocean measurements. The measurements of surface renewal at less energetic phases of the tidal cycle show a few orders of magnitude lower than the strongly wind-forced laboratory measurements. This suggests that at low wind speeds in the Parker River estuarine system surface renewal is driven by bottom-generated turbulence that is transported to the surface through the kinetic energy flux.

In the present study, near-surface turbulent dissipation rates ranged from 10^{-7} to 10^{-5} W kg^{-1} as shown in Fig. 5b. For comparison, estimates of near-surface ε using a microstructure profiler in the Hudson River near Manhattan ranged from 10^{-7} to 10^{-6} W kg^{-1} during neap tides and from 10^{-7} to 10^{-5} W kg^{-1} during spring tides (Peters and Bokhorst 2000). During that experiment, the peak Hudson River tidal flow was double that of the Parker River and exhibited half the tidal excursion. Since the mean depth of the Hudson River was roughly 15 m compared to only 2.5 m at the Parker River, comparable levels of ε are expected. The Parker River estuary typically is a weakly stratified system compared to the Hudson suggesting that the stratification does not play a significant role in the Parker River. In comparison to these estuarine systems, estimates of turbulent dissipation under breaking waves on Lake Ontario ranged from 10^{-5} to 10^{-2} W kg^{-1} (Agrawal et al. 1992; Terray et al. 1996) and energetic mixed layers show ε values from 10^{-6} to 10^{-4} W kg^{-1} (MacIntyre et al. 1995). This comparison suggests that the Parker River estuary exhibits near-surface dissipation levels similar to larger estuarine systems under comparably low wind speeds, but significantly less than that found under strongly wind-forced conditions. Our results demonstrate that turbulence that generates surface renewal is tidally forced under low wind conditions in the Parker River.

The measurements made during this study allow for an investigation of the various models that estimate the gas transfer velocity assuming differing governing processes. Commonly-used models for gas transfer in estuaries have been described that are based on wind speed (e.g., Raymond and Cole

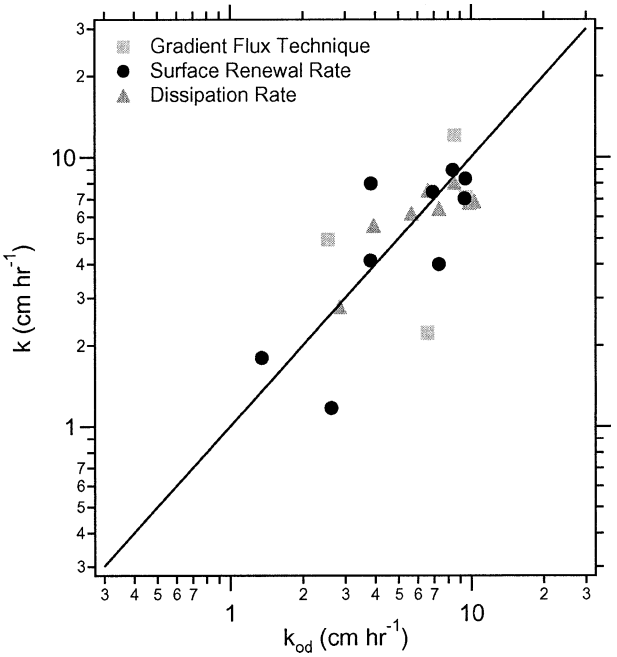

Fig. 8. Transfer velocities measured by the gradient flux technique, surface renewal theory, and the dissipation rate method versus k_{OD}, the transfer velocity determined using the O'Connor and Dobbins (1958) model. The model is calculated as $k_{OD} = 3.6 \times 10^5 (D_{O_2} V/H)^{0.5} (600/Sc_{O_2})^{0.67}$ where D_{O_2} and Sc_{O_2} are the diffusivity and the Schmidt number of oxygen, respectively.

2001), and water depth and flow speed (e.g., O'Connor and Dobbins 1958). Comparison of λ and ε with previous studies of energetic wind-forced systems and the results shown in Fig. 7 suggests that gas exchange on the Parker River under low winds may be tidally driven. Figure 8 shows the gas transfer velocity referenced to $Sc = 600$ (CO_2 at 20°C) determined from the gradient flux technique, surface renewal theory, and the turbulent dissipation rate versus k_{OD}, the gas transfer velocity determined from the O'Connor and Dobbins (1958) model for bottom-friction driven processes. Surface renewal theory predicts k from Eq. 6 using λ and is referenced to $Sc = 600$ using the relationship in Eq. 7. Lamont and Scott (1970) predict k in Eq. 3 using ε from the ID method. The choice of exponent n in Eqs. 3 and 7 depends on the cleanliness of the water surface and was set to $n = ⅔$ for a surfactant-influenced interface. All three methods correlate with the O'Connor and Dobbins (1958) model. The surface renewal (SR) and the dissipation rate (DR) estimates of k have correlation coefficients, R^2, of 0.75 and 0.74 respectively. The gradient flux technique measurements of k have an R^2 of 0.49 and visibly show more variability in Fig. 8 than the SR or the DR estimates. This is a consequence of the limited sampling as well as of the uncertainty in K_c in this low wind regime where the gradient flux technique may show more variability than actually exists (McGillis et al. 2001). Our data give quantitative support to the functional dependence of k based on both surface renewal theory in Eq. 2 and dissipation rate in Eq. 3. These are the first results to show that the gas transfer velocity varies significantly over a tidal cycle and that this variability is directly related to the turbulence and surface renewal at the air-water interface.

The choice of $n = ⅔$ for this study shows the best comparison of measurements to the model. This assessment is reasonable considering the potential sources for contamination of the water surface by surfactants from the neighboring marshes and the nearby marina. A dilemma with the DR method, the SR method using CFT, or any method that does not measure the specific gas of interest, is the importance placed on the choice of n to relate the measured passive scalar to the Schmidt number of the gas of interest. A choice of $n = ½$ would result in transfer velocities twice as high determined by the SR method and 3 times as high for the DR method. Therefore, independent determination of n is needed during future studies that attempt to develop a universal parameterization for k in estuaries. For the present study, the observed trends in Fig. 8 are not affected by the choice n and show that the gas transfer velocity is governed by tidally generated turbulence under low wind conditions in the Parker River.

Table 1 summarizes the estimates of k for this study referenced to $Sc = 600$. The results in Table 1 and Fig. 8 show that the three methods for k used in this study are in good agreement with the widely

TABLE 1. Average and range in transfer velocities corrected to a Schmidt number of 600 (k_{600}) for the measurements conducted during this field study on the Parker River under low wind conditions (1.9 ± 0.5 m s^{-1}) over a single tidal cycle.

Type of Measurement/Model	Range in k_{600} (cm hr^{-1})	Average k_{600} (cm hr^{-1})	Sample size
Gradient Flux Technique (This study)	2.2–12.0	6.6	4
Controlled Flux Technique (This study)	1.2–9.0	5.6	9
Dissipation Rate Technique (This study)	2.8–8.1	6.3	8
Water Depth and Flow Speed Model (River), O'Connor and Dobbins (1958)	1.4–10.3	6.4	21
Wind Speed Model (Estuary/River), Raymond and Cole (2001)	3.1–4.6	3.8	4

used river model of O'Connor and Dobbins (1958) in the trend, range and average value of k. Since the wind speed was low and constant during this study ($\sim$2 m s^{-1}), an estimate of k using the Raymond and Cole (2001) empirical relationship does not capture the variability observed over the tidal cycle and underestimates the measured k. The measurements of k from these three methods show variability relative to the O'Connor and Dobbins (1958) model. It is likely that the estimate of k from O'Connor and Dobbins (1958) does not completely capture the variability in gas transfer velocity due to the interplay between tidally- and wind-driven exchange. Though the transfer during this study appears to be tidally dominated, some fraction of the exchange may be explained through wind-driven exchange that is not captured by the model. The turbulence that produces surface renewal and promotes gas transfer is not solely generated at the bottom boundary. A component of the turbulence is generated through shear at the air-water interface, contributes to the overall transfer, and leads to variability in the model comparison. Therefore, the proper function for k in rivers and estuaries must consider tidal forcing as well as other processes, including wind.

Estimates of k from the SR and the DR methods compare well, suggesting that these estimates of k may prove to be useful in developing statistical models for gas exchange in estuaries that encompass the processes driving the transfer. The comparison with estimates of λ and ε to other systems, for example, shows that wind-forced systems have the potential to contribute significantly to, if not dominate, the forcing for gas exchange in estuaries. In particular, the direction of the wind speed could be significant when the near-surface shear generated during highly wind-forced events is modulated by the direction of the tidal currents. Shear will also be modulated by the sinuosity, or meandering, in rivers and estuaries where sharp bends cause eddies to form that may add turbulence to the MBL. Surfactants (Frew 1997), stratification, waves (Bock et al. 1999; Zappa et al. 2001b), and rain (Ho et al. 2000) are additional properties of the system other than tidal velocity, tidal height, wind speed, and sinuosity that effect near-surface turbulence and cause variability in k. The effects of surfactants and stratification are pronounced in rivers and estuaries and are of particular interest to explore. While the DR method captures the variability of k comparable to the SR method, the SR method may prove to be more powerful since it directly measures surface renewal by CFT whereas the DR method is applied at depth and may not capture the effects of surfactants on gas transfer that occur at the air-water interface. The turbulent dissipation rate measured at shallow depths also may be modified at the surface due to near-surface shear or stratification and lead to variability in k.

In this study, gas transfer measurements were developed and implemented over a tidal cycle to begin to understand the processes that produce the variability in k observed in rivers and estuaries. This work shows that gas transfer velocity over the course of a semi-diurnal tidal cycle at low wind speeds is driven by tidally-generated near-surface turbulence and surface renewal. Future studies will provide the ability to better determine all processes governing surface turbulence and k, to explore processes at higher wind speeds, and to incorporate the processes that are crucial in developing a river-estuary gas transfer model.

Conclusions

Measurements of k for CO_2 using the gradient flux technique were made from the mobile platform SPIP during a low wind period ($\sim$2 m s^{-1}) in order to focus on the effect of changes in tidal velocity on near-surface turbulence at the surface microlayer. These measurements of k were compared directly with measurements of turbulence (controlled flux technique and the dissipation rate method) and with models for k based on turbulent statistics and environmental factors controlling turbulence such as wind speed, tidal velocity and water depth. Infrared imagery showed considerable variability in the turbulent spatial and temporal scales that affect the interfacial boundary-layer transport processes, and this variability is consistent with the measurements of the surface renewal rate, λ, that ranged from 0.02 to 2 s^{-1} and turbulent dissipation rate, ε, that ranged from 10^{-7} to 10^{-5} W kg^{-1}. Measurements of k ranged from 2.2 to 12.0 cm hr^{-1} over a tidal cycle during low wind conditions and are shown to scale with tidal velocity as well as with the estimates of λ and ε. Tidal variability leads to significant variation in the near-surface turbulence (ε) that directly impacts surface renewal (λ) of the aqueous boundary layer, and therefore controls similar variations observed for the measured gas exchange. The observed correlation between the measurements of k by the gradient flux technique, CFT, and the DR method and the O'Connor and Dobbins (1958) model for k demonstrates that the variability in the gas transfer velocity under low wind conditions is governed by tidally-generated turbulence. The surface renewal rate and the turbulent dissipation rate have been used to model k in estuaries based upon the processes that are directly controlling gas flux across the air-water interface. This work provides fundamental information on determining the link-

ages between physical processes affecting the turbulence in the aqueous surface boundary layer that govern k and the spatial and temporal scales of gas flux in river and estuary systems. The results of this work are a step toward a more accurate prediction of k for any gas in river, estuary and potentially coastal systems with varying wind, tidal, stratification, and morphological regimes.

Acknowledgments

We wish to thank J. Kremer and an anonymous reviewer for their thoughtful and insightful critique of the original manuscript. The authors thank the Riverfront Marina of Rowley, Massachusetts, for their assistance and support during the fieldwork on the Parker River. Riverfront Marina provided covered staging space, technical assistance, and access to facilities and resources for the successful completion of this study. The authors thank A. Jessup and W. Asher of the Applied Physics Laboratory at the University of Washington for the use of their CO_2 laser. The authors thank C. Hopkinson, J. Vallino, and the Plum Island LTER for their generous support and commitment to this research. The authors also gratefully acknowledge support from the Rinehart Coastal Research Center at the Woods Hole Oceanographic Institution. This is a Woods Hole Oceanographic Institution contribution 10720.

Literature Cited

Agrawal, Y. C., E. A. Terray, M. A. Donelan, P. A. Hwang, A. J. Williams, III, W. M. Drennan, K. K. Kahma, and S. A. Kitaigorodskii. 1992. Enhanced dissipation of kinetic energy beneath surface waves. *Nature* 359:219–220.

Asher, W. E. and J. F. Pankow. 1986. The interaction of mechanically generated turbulence and interfacial films with a liquid phase controlled gas/liquid transport process. *Tellus, Series B* 38:305–318.

Bock, E. J., T. Hara, N. M. Frew, and W. R. McGillis. 1999. Relationship between air-sea gas transfer and short wind waves. *Journal of Geophysical Research* 104:25821–25831.

Businger, J. A., J. C. Wyngaard, Y. Izumi, and E. F. Bradley. 1971. Flux profile relationships in the atmospheric surface layer. *Journal of Atmospheric Sciences* 28:181–189.

Cerco, C. F. 1989. Estimating estuarine reaeration rates. *Journal of Environmental Engineering* 115:1066–1070.

Chu, C. R. and G. H. Jirka. 1995. Reaeration in combined wind/stream driven flows, p. 79–88. *In* B. Jähne and E. C. Monahan (eds.), Air-Water Gas Transfer. AEON Verlag and Studio, Hanau, Germany.

Clark, J. F., R. Wanninkhof, P. Schlosser, and H. J. Simpson. 1994. Gas exchange rates in the tidal Hudson river using a dual tracer technique. *Tellus* 46B:274–285.

Cole, J. J. and N. F. Caraco. 1998. Atmospheric exchange of carbon dioxide in a low-wind oligotrophic lake measured by the addition of SF6. *Limnology and Oceanography* 43:647–656.

Danckwerts, P. V. 1951. Significance of liquid-film coefficients in gas absorption. *Industrial and Engineering Chemistry* 43:1460–1467.

Donlon, C. J., T. J. Nightingale, T. Sheasby, I. S. Robinson, and W. J. Emery. 1999. Implications of the oceanic thermal skin temperature deviation at high wind speed. *Geophysical Research Letters* 26:2505–2508.

Donlon, C. J. and I. S. Robinson. 1997. Observations of the oceanic thermal skin in the Atlantic Ocean. *Journal of Geophysical Research* 102:18585–18606.

Dyer, A. J. 1974. A review of flux-profile relationships. *Boundary-Layer Meteorology* 7:363–372.

Edson, J. and C. W. Fairall. 1998. Similarity relationships in the marine atmospheric surface layer for terms in TKE and scalar variance budgets. *Journal of Atmospheric Sciences* 55:2311–2328.

Frew, N. M. 1997. The role of organic films in air-sea gas exchange, p. 121–172. *In* P. S. Liss and R. A. Duce (eds.), The Sea Surface and Global Change. Cambridge University Press, Cambridge, U.K.

Harriott, P. 1962. A random eddy modification of the penetration theory. *Chemical Engineering Science* 17:149–154.

Haußecker, H., S. Reinelt, and B. Jähne. 1995. Heat as a proxy tracer for gas exchange measurements in the field: Principles and technical realization, p. 405–413. *In* B. Jähne and E. C. Monahan (eds.), Air-Water Gas Transfer. AEON Verlag and Studio, Hanau, Germany.

Hill, R. H. 1972. Laboratory measurement of heat transfer and thermal structure near an air-water interface. *Journal of Physical Oceanography* 2:190–198.

Ho, D. T., W. E. Asher, L. F. Bliven, P. Schlosser, and E. L. Gordan. 2000. On the mechanisms of rain-induced air-water gas exchange. *Journal of Geophysical Research* 105:24045–24057.

Jähne, B. and H. Haußecker. 1998. Air-water gas exchange. *Annual Review of Fluid Mechanics* 14:321–350.

Jähne, B., P. Libner, R. Fischer, T. Billen, and E. J. Plate. 1989. Investigating the transfer processes across the free aqueous viscous boundary layer by the controlled flux method. *Tellus* 41B:177–195.

Jähne, B., K. O. Munnich, R. Bosinger, A. Dutzi, W. Huber, and P. Libner. 1987. On the parameters influencing air-water gas exchange. *Journal of Geophysical Research* 92:1937–1949.

Jessup, A. T., C. J. Zappa, M. R. Loewen, and V. Hesany. 1997. Infrared remote sensing of breaking waves. *Nature* 385:52–55.

Katsaros, K. B. 1977. The sea surface temperature deviation at very low wind speeds; Is there a limit? *Tellus* 29:229–239.

Katsaros, K. B. 1980. The aqueous thermal boundary layer. *Boundary-Layer Meteorology* 18:107–127.

Katsaros, K. B., W. T. Liu, J. A. Businger, and J. E. Tillman. 1977. Heat transport and thermal structure in the interfacial boundary layer measured in an open tank of water in turbulent free convection. *Journal of Fluid Mechanics* 83:311–335.

Lamont, J. C. and D. S. Scott. 1970. An eddy cell model of mass transfer into the surface of a turbulent liquid. *American Institute of Chemical Engineers Journal* 16:512–519.

Langbein, W. B. and W. J. Durum. 1967. The aeration of streams. U.S. Geological Survey Circular No. 542. U.S. Geological Survey, Reston, Virginia.

Ledwell, J. J. 1984. The variation of the gas transfer coefficient with molecular diffusivity, p. 293–302. *In* W. Brutsaert and G. H. Jirka (eds.), Gas Transfer at Water Surfaces. D. Reidel, Norwell, Massachusetts.

Liss, P. S. 1973. Processes of gas exchange across an air-water interface. *Deep-Sea Research* 20:221–238.

Liss, P. S. and L. Merlivat. 1986. Air–sea gas exchange rates: Introduction and synthesis, p. 113–127. *In* P. Buat-Ménard (ed.), The Role of Air–Sea Exchange in Geochemical Cycling. D. Reidel, Dordrecht, Holland.

Liss, P. S. and P. G. Slater. 1974. Flux of gases across the air-sea interface. *Nature* 247:181–184.

MacIntyre, S., R. Wanninkhof, and J. P. Chanton. 1995. Trace gas exchange across the air-water interface in freshwater and coastal marine environments, p. 52–97. *In* P. A. Matson and R. C. Harriss (eds.), Biogenic Trace Gases: Measuring Emissions from Soil and Water. Blackwell Scientific Publishing, Cambridge, Massachusetts.

McAlister, E. D. 1964. Infrared-optical techniques applied to oceanography I. Measurement of total heat flow from the sea surface. *Applied Optics* 3:609–612.

McAlister, E. D. and W. McLeish. 1969. Heat transfer in the top millimeter of the ocean. *Journal of Geophysical Research* 74: 3408–3414.

McAlister, E. D. and W. McLeish. 1970. A radiometric system for airborne measurement of the total heat flow from the sea. *Applied Optics* 9:2697–2705.

McGillis, W. R., J. W. H. Dacey, N. M. Frew, E. J. Bock, and R. K. Nelson. 2000. Water-air flux of dimethylsulfide. *Journal of Geophysical Research* 105:1187–1193.

McGillis, W. R., J. B. Edson, J. D. Ware, W. H. Dacey, J. E. Hare, C. W. Fairall, and R. Wanninkhof. 2001. Carbon dioxide flux techniques performed during GasEx-98. *Marine Chemistry* 75:267–280.

McKenna, S. P. and W. R. McGillis. 2001. Surface divergence and air-water gas transfer, p. 129–134. *In* M. A. Donelan, W. M. Drennan, E. S. Saltzman, and R. Wanninkhof (eds.), Gas Transfer at Water Surfaces. AGU Press, Washington, D.C.

O'Connor, D. and W. Dobbins. 1958. Mechanism of reaeration in natural streams. *Transactions of the American Society of Civil Engineers* 123:641–684.

Panofsky, H. A. and J. A. Dutton. 1984. Atmospheric Turbulence. J. Wiley and Sons, New York.

Peters, H. and R. Bokhorst. 2000. Microstructure observations of turbulent mixing in a partially mixed estuary. Part I: Dissipation rate. *Journal of Physical Oceanography* 30:1232–1244.

Raymond, P. A. and J. J. Cole. 2001. Gas exchange in rivers and estuaries: Choosing a gas transfer velocity. *Estuaries* 24:269–274.

Robinson, I. S., N. C. Wells, and H. Charnock. 1984. The sea surface thermal boundary layer and its relevance to the measurement of sea surface temperature by airborne and spaceborne radiometers. *International Journal of Remote Sensing* 5:19–45.

Saunders, P. M. 1967. The temperature at the ocean-air interface. *Journal of the Atmospheric Sciences* 24:269–273.

Schlüssel, P., W. J. Emery, H. Grassl, and T. Mammen. 1990. On the bulk-skin temperature difference and its impact on satellite remote sensing of sea surface temperature. *Journal of Geophysical Research* 95:13341–13356.

Smethie, W. M., T. Takahashi, D. W. Chipman, and J. R. Ledwell. 1985. Gas exchange and CO_2 flux in the tropical Atlantic Ocean determined from the ^{222}Rn and pCO_2 measurements. *Journal of Geophysical Research* 90:7005–7022.

Soloviev, A. V. and P. Schlüssel. 1994. Parameterization of the cool skin of the ocean and of the air-ocean gas transfer on the basis of modeling surface renewal. *Journal of Physical Oceanography* 24:1339–1346.

Soloviev, A. V. and P. Schlüssel. 1996. Evolution of cool skin and direct air-sea gas transfer coefficient during daytime. *Boundary-Layer Meteorology* 77:45–68.

Terray, E. A., M. A. Donelan, Y. C. Agrawal, W. M. Drennan, K. K. Kahma, I. A. J. Williams, P. A. Hwang, and S. A. Kitaigorodskii. 1996. Estimates of kinetic energy dissipation under surface waves. *Journal of Physical Oceanography* 26:792–807.

Vallino, J. J. and C. S. Hopkinson. 1998. Estimation of dispersion and characteristic mixing times in Plum Island Sound estuary. *Estuarine, Coastal and Shelf Science* 46:333–350.

Wanninkhof, R. 1992. Relationship between wind speed and gas exchange over the ocean. *Journal of Geophysical Research* 97:7373–7382.

Wanninkhof, R., W. Asher, R. Weppernig, H. Chen, P. Schlosser, C. Langdon, and R. Sambrotto. 1993. Gas transfer experiment on Georges Bank using two volatile deliberate tracers. *Journal of Geophysical Research* 98:20237–20248.

Wanninkhof, R. and W. R. McGillis. 1999. A cubic relationship between air-sea CO_2 exchange and wind speed. *Geophysical Research Letters* 26:1889–1892.

Watson, A. J., R. C. Upstill-Goddard, and P. S. Liss. 1991. Air-sea gas exchange in rough and stormy seas measured by a dual-tracer technique. *Nature* 349:145–147.

Wick, G. A., W. J. Emery, L. H. Kantha, and P. Schlüssel. 1996. The behavior of the bulk-skin sea surface temperature difference under varying wind speed and heat flux. *Journal of Physical Oceanography* 26:1969–1988.

Wilcock, R. J. 1984. Methyl chloride as a gas-tracer for measuring stream reaeration coefficients-II. *Water Research* 18:53–57.

Wu, J. 1971. An estimation of oceanic thermal-sublayer thickness. *Journal of Physical Oceanography* 1:284–286.

Zappa, C. J. 1999. Microscale wave breaking and its effect on air-water gas transfer using infrared imagery. Ph.D. Dissertation, University of Washington, Seattle, Washington.

Zappa, C. J., W. E. Asher, and A. T. Jessup. 2001a. Microscale wave breaking and air–water gas transfer. *Journal of Geophysical Research* 106:9385–9391.

Zappa, C. J., W. E. Asher, A. T. Jessup, J. Klinke, and S. R. Long. 2001b. Effect of microscale wave breaking on air-water gas transfer, p. 23–29. *In* M. A. Donelan, W. M. Drennan, E. S. Saltzman, and R. Wannikhof (eds.), Gas Transfer at Water Surfaces. AGU Press, Washington, D.C.

Zappa, C. J., A. T. Jessup, and H. H. Yeh. 1998. Skin-layer recovery of free-surface wakes: Relationship to surface renewal and dependence on heat flux and background turbulence. *Journal of Geophysical Research* 103:21711–21722.

Received for consideration, May 21, 2002
Revised, December 2, 2002
Accepted for publication, January 29, 2003